Simulations of the Freezing of Jet Fuel

J.S. Ervin[1], D. Atkins[1] and C. Obringer[2]
[1]University of Dayton Research Institute, 300 College Park
Dayton, OH 45469-0210, USA
[2]Air Force Research Laboratory, 1790 Loop Road N, Bldg 490
Wright-Patterson Air Force Base, OH 45433-7103, USA

Abstract

The objective of this research is to obtain images of the freezing of hydrocarbon fuels within a simple flow to assist understanding of the interaction between the flow and phase change dynamics. Another objective is to describe a computational model of the freezing process. JPTS, Jet A, and additized Jet A samples were cooled in a rectangular, aluminum chamber with quartz viewing windows. Images and surface temperatures were recorded during the solidification process. The images tracked the advancing freezing front and the influence of the buoyancy-driven flow. Cooling of JPTS resulted in the lowest volume of solids. When cooled, Jet A fuel containing a low-temperature additive exhibited a smaller solid volume than did the neat fuel. In addition, the additized Jet A fuel developed a population of suspended particles that was greater than that of neat Jet A fuel.

Introduction

High altitude flight can expose jet fuel in aircraft fuel tanks to temperatures below the freeze point temperature of commonly used fuels such as Jet A and JP-8. Freezing reduces fuel flow and solidified fuel can obstruct filters. If unchecked, fuel freezing may result in the loss of aircraft and crew. The U.S. Air Force has previously developed specialty fuels, such as JPTS, for low temperature use. Unfortunately, specialty fuels increase cost and logistical complexity. Commercial interest in the use of inexpensive fuels at low temperatures is increasing. For example, there is growing interest in high altitude commercial aircraft to provide high-speed broadband internet and cellular communication services[1]. Understanding the freezing of hydrocarbon jet fuels and the action of additives is necessary for the safe and economical operation of aircraft at high altitude.

Much past research has focused on aircraft fuel system operational issues. For example, in a NASA study[2], researchers examined the effects of heating jet fuel at low temperatures in a simulated fuel tank of complex geometry in an effort to improve fuel flowability. Unfortunately, photographs were not of sufficient resolution to distinguish between regions of liquid or solid fuel. For simplicity, fundamental studies of the freezing of hydrocarbons generally involve single compounds or binary mixtures. Unfortunately, jet fuel is a complex mixture of many hydrocarbons for which simple phase relationships do not exist. Clearly, more fundamental research is needed to better understand the freezing of jet fuel.

Computational simulations of the freezing process can assist in the fundamental understanding of freezing experiments. In addition, it is imperative for aircraft designers to have computational tools which can simulate the freezing process within fuel systems. This paper describes a computational model of the

Paper presented at the RTO AVT Symposium on "Advanced Flow Management: Part B – Heat Transfer and Cooling in Propulsion and Power Systems", held in Loen, Norway, 7-11 May 2001, and published in RTO-MP-069(I).

Report Documentation Page

Form Approved
OMB No. 0704-0188

1. REPORT DATE	2. REPORT TYPE	3. DATES COVERED
00 MAR 2003	**N/A**	**-**

4. TITLE AND SUBTITLE	5a. CONTRACT NUMBER
Simulations of the Freezing of Jet Fuel	5b. GRANT NUMBER
	5c. PROGRAM ELEMENT NUMBER
6. AUTHOR(S)	5d. PROJECT NUMBER
	5e. TASK NUMBER
	5f. WORK UNIT NUMBER
7. PERFORMING ORGANIZATION NAME(S) AND ADDRESS(ES) **NATO Research and Technology Organisation BP 25, 7 Rue Ancelle, F-92201 Neuilly-Sue-Seine Cedex, France**	8. PERFORMING ORGANIZATION REPORT NUMBER
9. SPONSORING/MONITORING AGENCY NAME(S) AND ADDRESS(ES)	10. SPONSOR/MONITOR'S ACRONYM(S)
	11. SPONSOR/MONITOR'S REPORT NUMBER(S)

12. DISTRIBUTION/AVAILABILITY STATEMENT
Approved for public release, distribution unlimited

13. SUPPLEMENTARY NOTES
Also see ADM001490, presented at RTO Applied Vehicle Technology Panel (AVT) Symposium held in Leon, Norway on 7-11 May 2001, The original document contains color images.

14. ABSTRACT

15. SUBJECT TERMS

16. SECURITY CLASSIFICATION OF:			17. LIMITATION OF ABSTRACT	18. NUMBER OF PAGES	19a. NAME OF RESPONSIBLE PERSON
a. REPORT	b. ABSTRACT	c. THIS PAGE			
unclassified	**unclassified**	**unclassified**	**UU**	**12**	

Standard Form 298 (Rev. 8-98)
Prescribed by ANSI Std Z39-18

freezing of jet fuel. Another objective of this study is to obtain detailed images of jet fuel freezing within a buoyancy-induced flow with imposed surface temperatures. The present experiments use well-defined temperature conditions and a rectangular geometry that provides a two-dimensional flow. Neat fuels and fuels blended with additives are subjected to an imposed cooling rate. Recorded images assist the understanding of how fluid dynamics influence phase change and how additives modify fuel crystallization.

Experimental

Figure 1 shows a schematic of the test apparatus. For simplicity, a rectangular geometry was chosen for the optical freezing cell. The aluminum cell (88.9 mm x 38.1 mm x 44.5 mm) has a wall thickness of 6.4 mm. Copper block heat exchangers are clamped to opposite vertical sides of the optical cell to create temperature differences in the fuel, and the resulting density differences drive the flow within the cell. A passage within each block permitted liquid nitrogen flow. Control of the temperature (within $\pm$0.5 ^{o}C) of each copper block was accomplished by the use of cryogenic solenoid valves which metered the flow of liquid nitrogen. Calibrated (type T) thermocouples (estimated uncertainty of $\pm$0.5 °C) were used to measure temperatures on the surfaces of the aluminum cell. Polarizing filters were used to enhance the contrast between the liquid and solid fuel.

Each fuel was subjected to the surface temperatures shown in Figure 2. The cooling experiment was divided into three periods. For convenience, during the first period (Figure 2, A-B), the lower-temperature surface (T_L) was cooled rapidly from room temperature (293.2 K) at a rate of 5.0 K/min. During the second period (Figure 2, B-C), the lower-temperature surface (T_L) was cooled from 243.2 K to 208.2 K at a rate of 1.0 K/min. To ensure freezing T_L was set at 208.2 K, which is less than the lowest pour point temperature of the fuels studied (Table 1). A 15 K temperature difference between the opposite vertical surfaces was maintained throughout the experiment to induce flow. The vertical surfaces were then maintained at constant temperatures (Figure 2, C-F) for a period of fifteen minutes. Top and bottom surface temperatures of the cell were not actively controlled, but were measured. Details of the experimental procedure and apparatus appear in reference 3.

JPTS (F3775), Jet A (F3219), and Jet A additized (2000 mg/L) with a proprietary low-temperature additive (F3607) were selected for study. Table 1 lists select low-temperature properties of the fuels. Before freezing, the samples were analyzed using gas chromatography to determine the n-alkane (weight) distribution. The JPTS sample consists of 33% n-alkanes ranging from C_8 to C_{15} and centered about C_{11}. The Jet A sample has 24% n-alkanes in the range C_8 to C_{17} and centered about C_{12}. The Jet A sample contains the greatest mass of long-chain n-alkanes (C_{15}-C_{17}).

Model

Although this paper focuses on low-temperature experiments, it is appropriate to describe a model which will be used in the simulations of freezing fuel. In our model, the liquid and solid phases are not considered separately, and a mushy zone is assumed to exist between the solid and liquid phases. The flow within the mushy region is treated in terms of an effective resistance quantity A:

$$A \sim \frac{-C\left(1-\lambda\right)^2}{\left(\lambda^3+q\right)} \tag{1}$$

Similar forms of an effective resistance within the mushy region have been successfully applied in the study of metal alloys[4]. λ in the above equation is a function of the characteristic diameter (d_s) of the solid crystals and the solid volume fraction, ε_s. Here, ε_s is found from solution of the enthalpy equation and additional property characteristics obtained from differential scanning calorimetry and microscopic measurements. In addition, the d_s and ε_s for jet fuel can be estimated from images of freezing jet fuel. A may be incorporated in the momentum equations, and a limiting value of A (~ $-C/q$) can be chosen to be large enough to eliminate velocities in the solid:

$$\frac{\partial(u\rho)}{\partial t}+\frac{\partial(uu\rho)}{\partial x}+\frac{\partial(vu\rho)}{\partial y}=\nabla\bullet(\mu\nabla u)-\frac{\partial P}{\partial x}-Au \tag{2}$$

$$\frac{\partial(v\rho)}{\partial t}+\frac{\partial(uv\rho)}{\partial x}+\frac{\partial(vv\rho)}{\partial y}=\nabla\bullet(\mu\nabla v)-\frac{\partial P}{\partial y}-Av+\rho f_y \tag{3}$$

where ρf_y represents the gravitational body force effect. Transport properties are treated as a linear function of the local solid fraction, and the flow is assumed to be two-dimensional, laminar, and incompressible. In addition, the solid phase is at rest, and the density change resulting from phase change is negligible. The fuel is represented by a single compound because it is impractical to model the multitude of compounds present in jet fuel. An iterative finite difference (fixed grid) solution of the conservation equations can be performed over the entire liquid/solid region using an enthalpy equation that is similar to the single-phase enthalpy equation[5].

Results and Discussion

Surface temperatures and the temperature at the center of the optical cell are presented for each fuel sample (Figure 2). In addition, images (Figures 3-8) are presented for each fuel sample at the times and surface temperatures indicated in Figure 2 (times C, D, E and F).

Temperature Measurements. Figure 2 shows temperature readings at the center of the optical cell as well as the temperatures imposed on the vertical surfaces of the optical cell for all the fuel samples. Since the fuel samples possess different thermal and transport properties, the center temperature differs between samples. Figure 2 shows the temperatures at which phase change was visually observed to begin on the lower-temperature surface for the JPTS and Jet A (neat and additized) samples. Figure 2 also shows that after phase change begins, the center temperatures begin to deviate from each other due to surface freezing and concomitant heat release due to crystallization.

Optical Cell Images. Figure 3 shows images of the JPTS sample freezing. In Figure 3, the right side of each image is the lower-temperature surface, and the left side is the higher-temperature surface. The surface temperatures for each image of the figure correspond to times C, D, E and F shown in Figure 2. Figure 3(a) shows fuel that has begun to solidify after 45 minutes of cooling (Figure 2, A-C). The light region of Figure 3(a) is fuel that has solidified on the lower-temperature vertical surface and the top and bottom surfaces. The remaining area is liquid that appears dark due to the cross-polarization used. Figures 3(a)-3(d) show that with increasing time, the crystallization front advances along the bottom and top of the cell from the lower-temperature vertical surface toward the higher-temperature vertical surface. After 60 minutes of cooling, the solidifying structure has advanced to the center of the top and bottom surfaces, and a profile of the solidified structure is visible. The profile extends uniformly from the front to the rear of the cell, indicating that heat transfer end effects are negligible and the buoyancy-driven flow field is two-dimensional. The images in Figure 3 suggest that the solidifying structure is comprised of long, thin crystals, adhered to the cell surfaces. The thickest portion of the solidifying structure is located at the bottom of the lower-temperature surface (Figure 3(d)).

Figure 4(a) shows the JPTS sample in the optical cell after 60 minutes of cooling with a (6.4 mm) uniform grid superimposed. The profile area of the stationary solidified fuel attached to the cell surfaces is estimated from this image to be 594 mm^2. From this area, it can be estimated that the solidifying structure occupies 18% of the optical cell volume. Figure 4(b) (10X magnification) reveals a porous structure of needle-like crystals, generally growing in the opposite direction of the heat transfer (normal to the cell surfaces). The needle-like crystals visible in Figure 4(b) have a characteristic width of 0.1 mm and reach lengths equivalent to the thickness of the solidifying structure (6 mm). Crystal spacing varies, but distances as great as 1 mm can be measured between crystals.

Figure 5 shows images of Jet A freezing while holding surface temperatures constant (Figure 2, C-F). Figure 5(a) shows that after 45 minutes, a crystalline structure covers the vertical lower-temperature

surface and the top and bottom surfaces. It is obvious that Jet A crystal morphology is very different from that of the JPTS sample. Figure 5 shows that components of the fuel solidify and attach to the surfaces of the optical cell. In addition, crystals nucleate and drift within the liquid. As time progresses, the liquid fuel temperature falls below the cloud point throughout the cell, and the suspended crystals continue to grow. The crystals move with convective currents, becoming entangled with the surface-adhered crystalline structures. There, they pack and contribute to the growth of the adhered, larger structures. Thus, the buoyancy-induced flow creates a mechanism for growth of stationary crystalline structures. After 60 minutes, Figure 5(d) shows all surfaces have adhering crystals with the greatest accumulation of solids at the bottom of the cell, as observed with the JPTS sample. The thickness of the crystalline structure exceeds 12 mm along portions of the vertical lower-temperature and bottom surfaces. Areas of solidification adjacent to the cell surfaces are dark.

Figures 6(a) and 6(c) (10X magnification) reveal the neat Jet A sample crystal habit and the growth mechanism of the larger structures. Figure 6(a) shows migrating crystals become attached to surface adhered crystals. Figure 6(c) shows densely packed crystals that have adhered to the lower-temperature vertical surface with no identifiable spacing between crystals. Closer inspection of Figure 6(c) shows that the crystals are randomly oriented. Figure 6(b) shows Jet A in the optical cell after 60 minutes. The area of solidification is more difficult to estimate than for the other fuels since numerous suspended crystals are present in the liquid region. However, it is estimated from Figure 6(b) that the solidified fuel attached to the cell surfaces occupies 47% of the cell volume. Figure 6(c) shows the stationary crystalline structures to be made up of short, uniform plate-like crystals, packed together randomly, accumulating in a direction opposite that of the heat transfer. As the solid fraction increases in the cell, the crystal interaction increases, causing packing and formation of larger, stationary solid structures. Figure 6(a) shows these crystals to be 0.1 mm thick and 1 mm in length. Figure 6(c) shows densely packed crystals in the dark region adjacent to the lower-temperature surface. It is believed that the dark regions are relatively non-porous solid structures.

The motion of the liquid fuel influences the local liquid temperature, which, in turn, affects the crystal growth rate and habit. The buoyancy-induced flow driven by the imposed surface temperatures affects the growth of solidifying structures. Large-scale liquid motion flows downward along the lower-temperature vertical surface and upward along the higher-temperature vertical surface in a clockwise rotation. Thus, the minimum temperature of the flowing liquid is located near the bottom of the vertical lower-temperature surface. As observed in the present experiments, this region would be expected to have the greatest accumulation of solidified fuel.

Analysis of the n-alkane species before freezing assists the understanding of crystallization. JPTS is the present preferred low-temperature jet fuel as the freeze point temperature of JPTS is lower than that of the Jet A fuel. Yet, the JPTS fuel contains the greatest mass of n-alkanes (32%). The Jet A fuel contains a

greater mass of larger n-alkane species (C_{15}-C_{16}) than the JPTS, which may account for the higher freeze point temperature of the Jet A sample.

The crystallization behavior of the JPTS sample (long, needle-like crystals, attached to the cell walls) has been observed in metal alloy solidification and is referred to as columnar (constrained) dendritic solidification[6]. In addition, the crystal formation and subsequent interaction exhibited in the present study by Jet A has similarly been observed in alloy solidification and is referred to equiaxed (unconstrained) crystallization[6]. Thus, the crystallization behavior of the hydrocarbons contained in JPTS and Jet A is similar to that observed in metal alloy solidification. It is believed that numerical models used in the simulation of alloy solidification may be extended to the freezing of jet fuel. Moreover for modeling the freezing of jet fuel, the optical cell images can provide estimates of d_s and ε_s.

Additive Studies. Previous research involved the evaluation of the effectiveness of cold flow additives to reduce the amount of fuel trapped by the solidifying wax structure[7]. Proprietary additive F3607 was found to be effective and is used in the present experiments.

Figure 7 shows images of freezing Jet A additized with (2000 mg/L) F3607 in the period from 45 to 60 minutes (Figure 2, C-F). Figure 7(d) shows that there are a greater number of smaller crystals than were present in the neat Jet A sample (Figure 5(d)) for otherwise identical conditions. When compared to the neat Jet A sample (Figure 5), the crystals in the solidifying structure are neither as densely packed nor attached to the cell surfaces. Figure 7 shows that the additive has significantly altered the crystal habit of Jet A, revealing why the additive was effective. The migrating equiaxed crystals do not densely pack, but migrate to the bottom of the cell, and the accumulated crystals shift with liquid fuel flow. Figure 8(a) and 8(c) (10X magnification) reveal small, irregularly shaped crystals that do not densely pack. Also, the magnified images show the crystals are needle-like in shape as opposed to the plate-like crystals observed in the solidifying neat Jet A. The length of these needle-like crystals (0.5 mm) are roughly half the length of the plate-like neat Jet A crystals (1 mm), while crystal thickness is similar (<0.1 mm). Figure 8(b) shows the optical cell at 60 minutes. As with neat Jet A, the volume of solidification is difficult to estimate, roughly 40% of the optical cell volume.

Using differential scanning calorimetry[8], the onset of phase change was determined (Table 1) at a 1.0 K/min cooling rate for the fuels of the present work. Under the thermal conditions of the optical cell, the wall temperature at which crystallization initially becomes visible corresponds well to the differential scanning calorimetry measurements and to the measured cloud-point temperatures. This agreement among different studies supports the experimental method of the present work.

Conclusions

Images of JPTS, Jet A, and additized Jet A jet fuels freezing within a buoyancy-induced, two-dimensional flow were obtained using an optical cell. Buoyancy-induced flow controlled the growth of fuel crystals on the chamber walls. In addition, the flow enhanced the growth of solid structures on wall

surfaces for the Jet A sample by increasing crystal interaction. The effective additive did not substantially change the amount of solid formation, but changed crystal shape, size, and packing. Additives that create irregularly shaped, needle-like crystals are effective cold flow additives because the resulting crystal habits are permeable to flow. The images recorded provide sufficient resolution to estimate characteristic crystal sizes of the solidifying structures for computational modeling. Moreover, experiments which employ well-defined thermal conditions and simple geometries assist the understanding of how hydrocarbon fuels freeze. The optical cell experiments suggest that jet fuels with a wide distribution of small n-alkane species ($<C_{14}$) may have desirable low temperature properties.

Acknowledgements

This work was supported by the U.S. Air Force, Warner Robins Air Logistic Command, U-2 Special Programs Office, Robins Air Force Base, Warner Robins, Georgia, under Project No. 205 (Project Manager: Doug Hanlin) and the U.S. Air Force Research Laboratory, Propulsion Directorate, Propulsion Sciences and Advanced Concepts Division, Wright-Patterson Air Force Base, Ohio, under Contract No. F33615-97-C-2719 (Technical Monitor R. Morris). We would like to thank R. Striebich for the gas chromatograph analysis, N. Widmor for the differential scanning calorimetry measurements, and Lt. K. Wohlwend (USAF) for the freeze point, pour point, and cloud point measurements.

References

(1) Iannotta, B., *Aerospace America*. 2000, *40*, 36-40.
(2) Stockmer, F. J., "Experimental Study of Fuel Heating at Low Temperatures in a Wing Tank Model: Final Report-Volume I", NASA CR 165391, 1981.
(3) Atkins, D., Ervin, J.S., Vangsness, M., and Obringer, C., "*Flow Visualization of the Freezing of Jet Fuel*" Proceedings of the 7th Intl. Conf. On Stability and Handling of Liquid Fuels, Graz Austria, 2000.
(4) Ni, J.; Incropera, F. P. *Int. J. Heat Mass Transfer*. 1995, 38, 1271-1284.
(5) Sasaguchi, K.; Kusano, K.; Viskanta, R; R. *Int. J.Heat Mass Trans.* 1997, 40, 1343-1354.
(6) Beckermann, C.; Viskanta, R. *ASME Appl Mech Rev,* 1983, 46, 1-25.
(7) Ervin, J. S.; Zabarnick, S.; Binns, E.; Dieterle, G.; Davis, D.; Obringer, C. *Energy & Fuels*. 1999, 13, 1246-1251.
(8) Ervin, J. S.; Widmor, N.; Zabarnick, S. *"Studies of Jet Fuel Freezing by Differential Scanning Calorimetry and Cold-Stage Microscopy", ASME Turbo Expo*. New Orleans, June 2001.

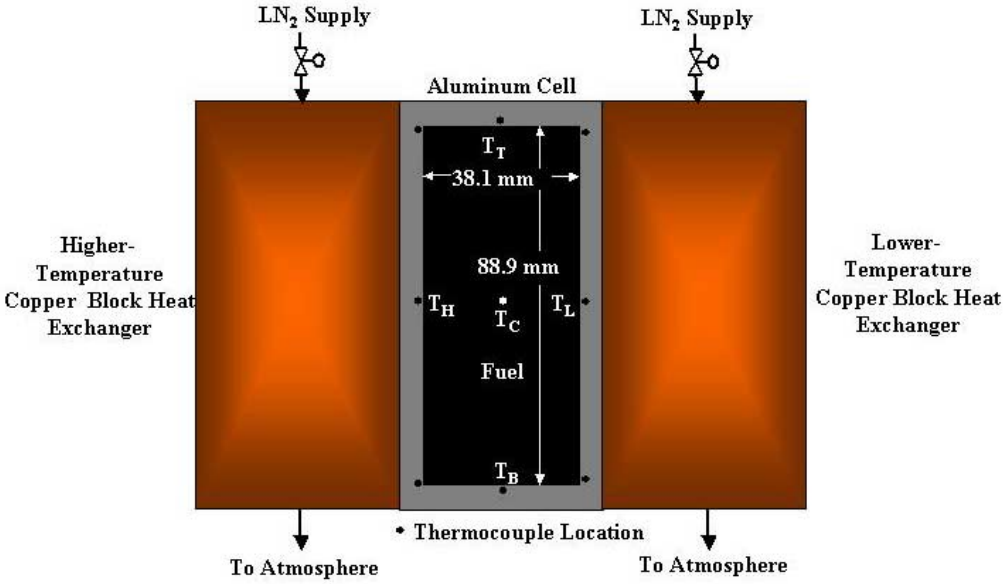

Figure 1. Schematic of low-temperature optical cell.

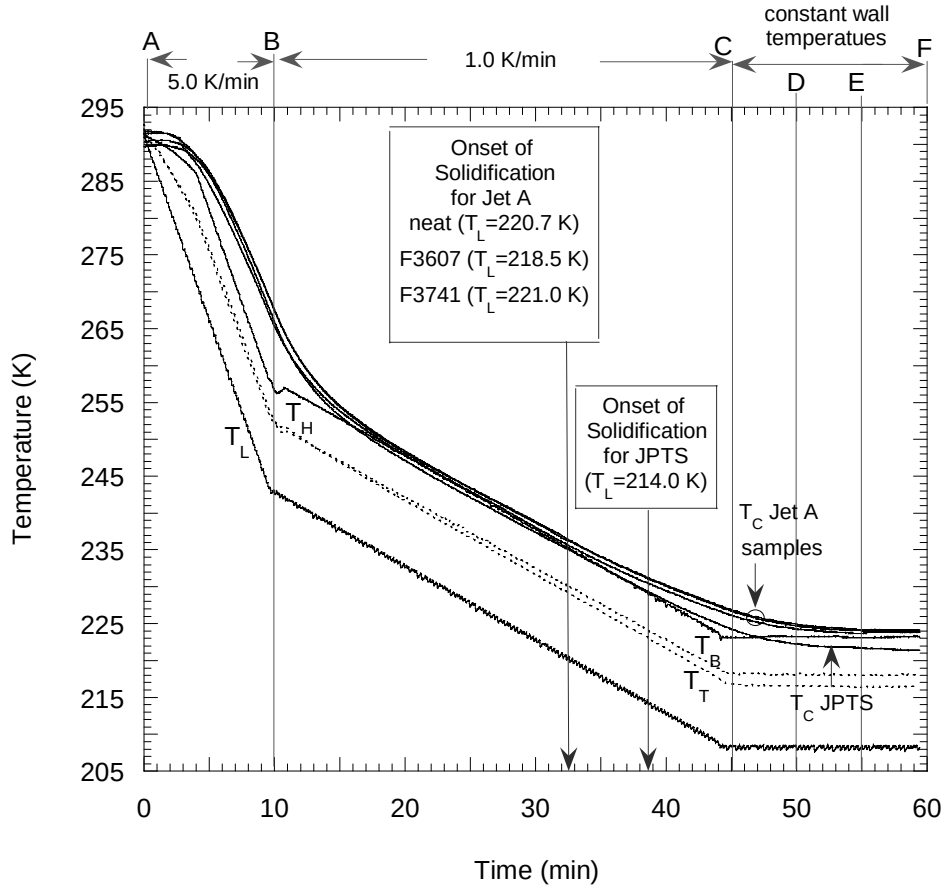

Figure 2. Optical cell surface and center temperatures for all fuel samples.

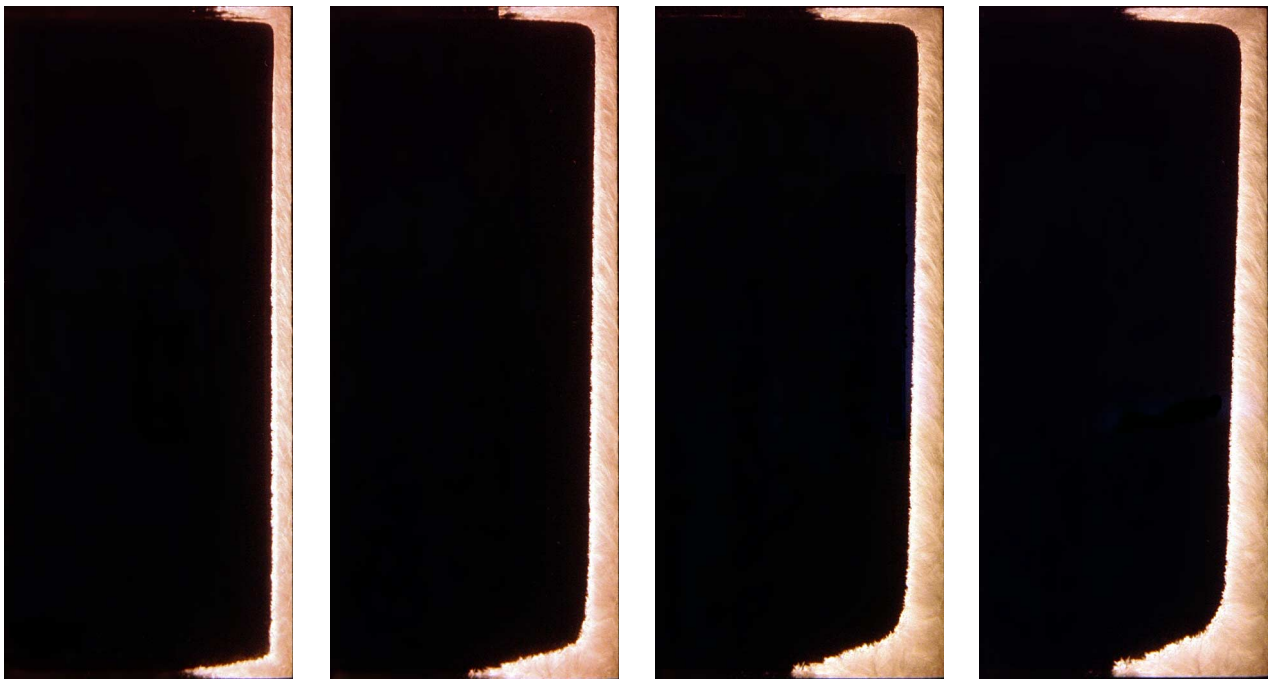

(a) (b) (c) (d)

Figure 3. Freezing JPTS after (a) 45 minutes (b) 50 minutes (c) 55 minutes (d) 60 minutes of cooling in the optical cell. Times refer to those of Figure 2.

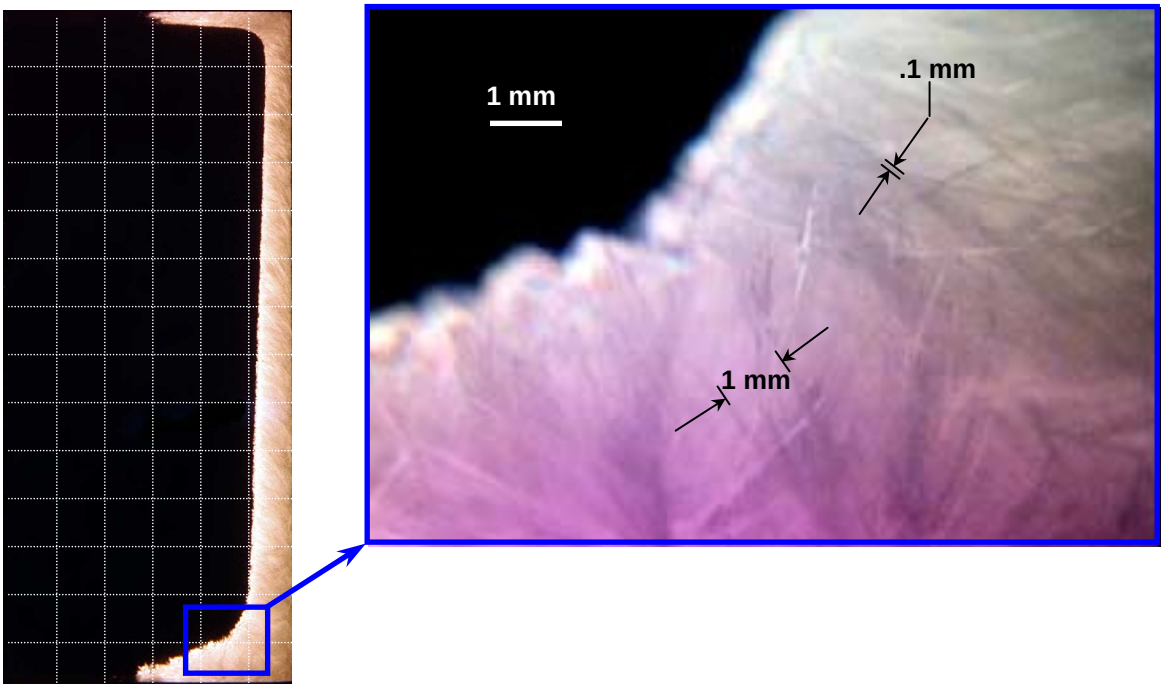

(a) (b)

Figure 4. Frozen JPTS (a) 594 mm^2 of solidified fuel and (b) crystal habit after 60 minutes of cooling.

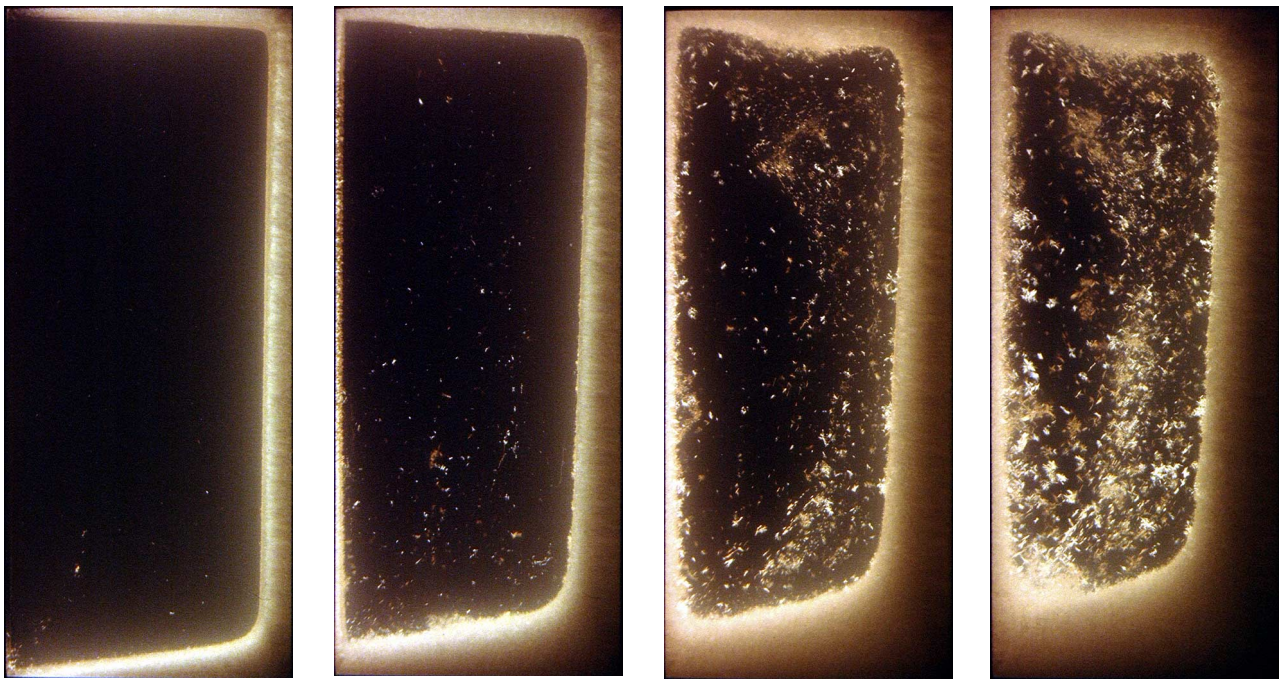

(a) (b) (c) (d)

Figure 5. Freezing Jet A after (a) 45 minutes (b) 50 minutes (c) 55 minutes (d) 60 minutes of cooling in the optical cell. Times refer to those of Figure 2.

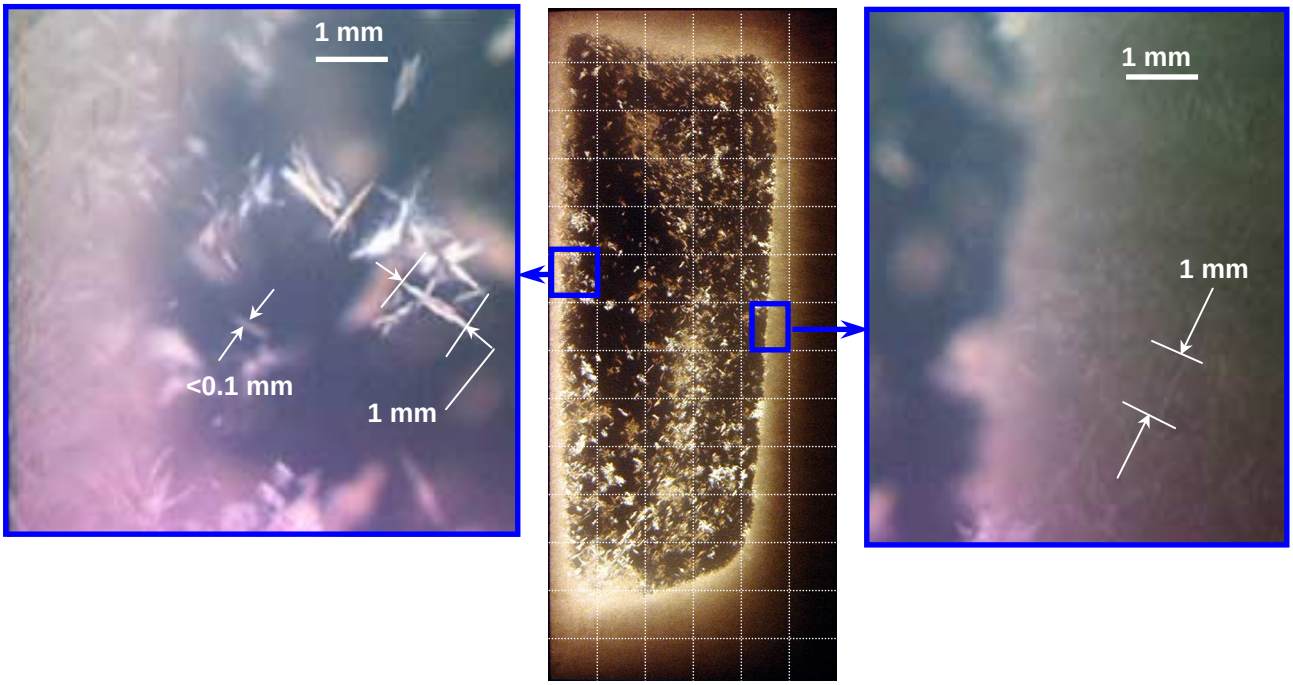

(a) (b) (c)

Figure 6. Frozen Jet A (a) crystal habit, (b) 1594 mm^2 of solidified fuel area and (c) densely packed crystals after 60 minutes of cooling.

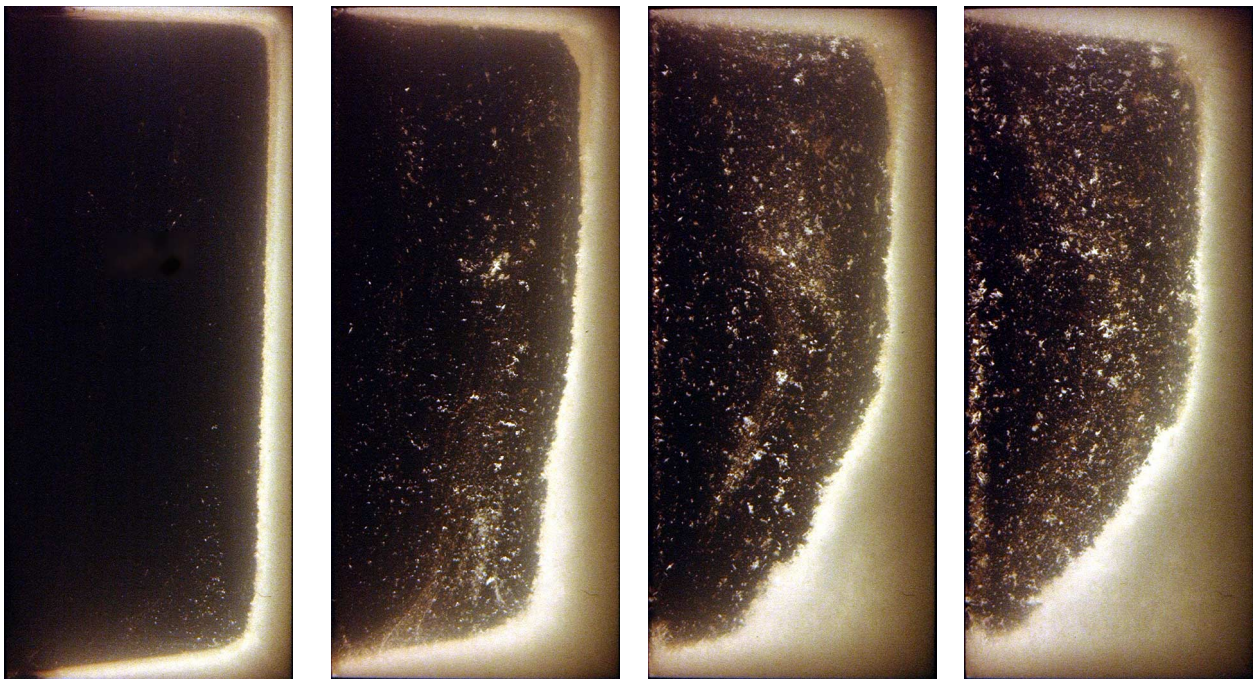

(a) 45.0 Minutes (b) 50.0 Minutes (c) 55.0 Minutes (d) 60.0 Minutes

Figure 7. Freezing Jet A additized with F3607 after (a) 45 minutes (b) 50 minutes (c) 55 minutes (d) 60 minutes of cooling in the optical cell. Times refer to those of Figure 2.

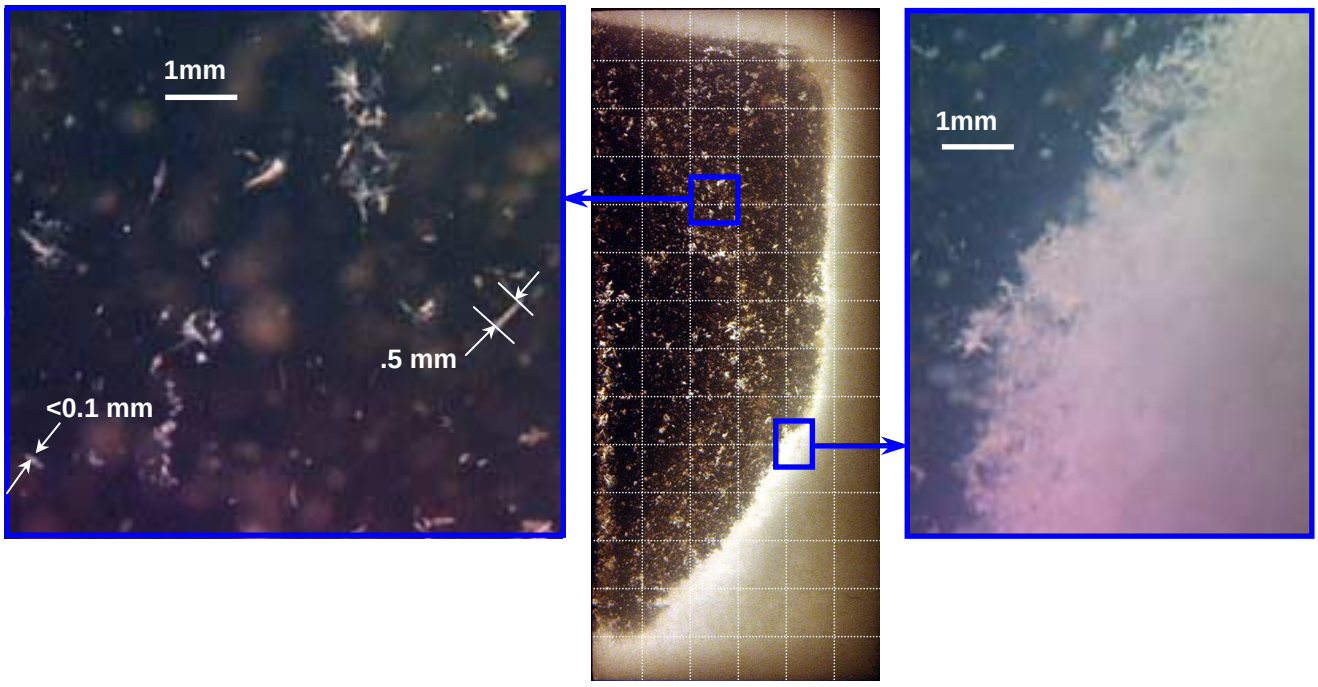

(a) (b) (c)

Figure 8. Frozen Jet A additized with F3607 (a) crystal habit, (b) 1361 mm^2 of solidified fuel and (c) migrating crystals after 60 minutes of cooling.

Table 1. Select Low-Temperature Properties of Fuels Studied and Comparison of Onset of Phase Change.

Fuel	*Freeze Point (K)*	*Cloud Point (K)*	*Pour Point (K)*	*Cell Onset-T_L (K)*	*DSC Onset (K)*
JPTS (F3775)	218.7	215.9	212.2	214.0	214.6
Jet A (F3219)	227.2	222.2	217.2	220.5	222.2
Jet A (F3219 additized with F3607)	227.2	222.3	208.3	218.5	221.2
Jet A (F3219 additized with F3741)	228.4	221.2	211.2	221.0	219.0